Geosci. Model Dev. Discuss., 6, 4417–4445, 2013
www.geosci-model-dev-discuss.net/6/4417/2013/
doi:10.5194/gmdd-6-4417-2013

Geoscientific Model Development Discussions
Open Access

Can sparse proxy data constrain the strength of the Atlantic meridional overturning circulation?

T. Kurahashi-Nakamura[1], **M. Losch**[2], **and A. Paul**[1]

[1]MARUM – Center for Marine Environmental Sciences and Faculty of Geosciences, University of Bremen, Bremen, Germany
[2]Alfred Wegener Institute for Polar and Marine Research, Bremerhaven, Germany

Received: 17 July 2013 – Accepted: 29 July 2013 – Published: 20 August 2013

Correspondence to: T. Kurahashi-Nakamura (tkurahashi@marum.de)

Published by Copernicus Publications on behalf of the European Geosciences Union.

Abstract

In a feasibility study, the potential of proxy data for the temperature and salinity during the Last Glacial Maximum (LGM, about 19 000 to 23 000 yr before present) in constraining the strength of the Atlantic meridional overturning circulation (AMOC) in a general ocean circulation model was explored. The proxy data were simulated by drawing data from four different model simulations at the ocean sediment core locations of the Multi-proxy Approach for the Reconstruction of the Glacial Ocean surface (MARGO) project and perturbing these data with realistic noise estimates. The results suggest that our method has the potential of providing estimates of the past strength of the AMOC even from sparse data, but in general paleo-sea surface temperature data without additional prior knowledge about the ocean state during the LGM is not adequate to constrain the model. On the one hand, additional salinity data in the deep ocean and at the sea surface are shown to be highly important in estimating the LGM circulation and as expected, reducing proxy-data errors improves the solutions. Whereas increasing the amount of surface data alone does not appear to be enough for better estimates. Finally, better initial guesses to start the state estimation procedure from greatly improve the performance of the method. Indeed, with a sufficiently good first guess, just the sea-surface temperature data from the MARGO project appear sufficient for reliable estimates of the strength of the AMOC.

1 Introduction

The ocean is an important component of the climate system because of its large storage and transport of heat and its strong control on the atmospheric circulation. To understand the dynamics of climate change, it is essential to assess the role of the ocean. Proxy evidence (e.g., Keigwin and Lehman, 1994; Clark et al., 2001; Epica Community Members et al., 2006) and climate models (e.g., Ganopolski and Rahmstorf, 2001; Stocker and Johnsen, 2003) suggest close links between the temperature

GMDD
6, 4417–4445, 2013

in the Atlantic region and variations of the Atlantic meridional overturning circulation (AMOC) and North Atlantic Deep Water (NADW) formation during past climate changes such as Dansgaard–Oeschger and Heinrich events. Associated changes in the ventilation of the deep ocean presumably affected the global climate by reorganising the cycling of carbon and other nutrients, which in turn led to different concentrations of carbon dioxide (CO_2) in the atmosphere (e.g., Archer, 1991; Archer et al., 2000; Gildor and Tziperman, 2001; Schulz et al., 2001; Kurahashi-Nakamura et al., 2010). Therefore, proper reconstructions of the AMOC and the formation of NADW are key elements in understanding the climate dynamics in the past.

The Last Glacial Maximum (LGM, 19 000–23 000 yr before present, Mix et al., 2001) is one of the most suitable time periods for studying a climate that is very different from the modern one, because the data coverage for the LGM is comparatively good, and the radiative forcings, boundary conditions and climate response are relatively well known Solomon et al. (2007). Nevertheless, the ocean circulation during the LGM is uncertain to the extent that even the question whether the strength of the AMOC and the rate of formation of NADW was larger or smaller in the LGM than in the modern day climate is still open to debate.

For example, a weaker AMOC or lower rate of NADW formation is inferred by Lynch-Stieglitz et al. (1999a, b) and Lynch-Stieglitz et al. (2006) based on a geostrophic transport estimate for the Florida Current from the oxygen isotope ratio $^{18}O/^{16}O$ recorded in the fossil shells of benthic foraminifera (often expressed as the deviation from a standard $\delta^{18}O$), by Piotrowski et al. (2005) based on neodymium ($^{143}Nd/^{144}Nd$) isotope ratios and by McManus et al. (2004) and Negre et al. (2010) based on north-to-south gradients of rate-sensitive radiogenic $^{231}Pa/^{230}Th$ isotope ratios (these authors even argue for a reversal of the abyssal flow during the LGM).

In contrast, a stronger AMOC or higher rate of NADW (or so-called GNAIW – Glacial North Atlantic Intermediate Water) formation is hypothesised by Yu et al. (1996) and Lippold et al. (2012) also based on $^{231}Pa/^{230}Th$ isotope ratios, by McCave et al. (1995); Manighetti and McCave (1995) and McCave and Hall (2006) based on the grain-size

GMDD
6, 4417–4445, 2013

analysis of ocean sediments, and by Curry and Oppo (2005) based on the stable carbon ($^{13}C/^{12}C$) isotope ratios and cadmium/calcium (Cd/Ca) trace element ratios.

Finally, Rutberg and Peacock (2006) interpret $\delta^{13}C$ records as consistent with a circulation regime similar to today.

Estimates of the NADW formation rate for the LGM by various numerical climate models with common forcings and boundary conditions also are not consistent with each other (cf. Otto-Bliesner et al., 2007). On the other hand, limited numbers of studies utilised a data assimilation technique for the state estimation of the AMOC in the LGM. Winguth et al. (1999) and Winguth et al. (2000) assimilated the $\delta^{13}C$ and Cd/Ca data into a global ocean model and suggested shallower and about 30 % weaker NADW formation with an adjoint ocean model (Winguth et al., 2000). Dail (2012) used the sea-surface temperature (SST) data by the MARGO project (Margo Project Members et al., 2009), $\delta^{13}C$ and $\delta^{18}O$ for state estimation in the Atlantic domain, and inferred that the NADW in the LGM was shallower but as strong as in the modern day.

More direct indicators of the past NADW formation rate would be the temperature and salinity of seawater, because they are the basic physical properties that define the water masses. Since temperature and salinity drive the ocean circulation through density differences, a numerical ocean model could be used to quantify an ocean circulation that is consistent with the temperature and salinity data.

To date, the most comprehensive compilation of SST estimates for the LGM ocean is provided by the MARGO project (Margo Project Members et al., 2009). A similar data set for sea-surface salinity does not yet exist. Local estimates of the salinity of LGM bottom water may be obtained from measurements of the $\delta^{18}O$ of the pore fluid in seafloor sediments (Adkins et al., 2002), but there is no direct proxy for salinity that could be applied generally. The $\delta^{18}O$ of planktonic foraminifera depend on the local salinity as well as on temperature, and thus it is possible to estimate the salinity if one can remove the temperature effect with the help of an independent temperature proxy such as the Mg/Ca ratio (Gebbie and Huybers, 2006). However, error propagation yields large errors on the reconstructed salinity (Schmidt, 1999; Rohling, 2000).

GMDD
6, 4417–4445, 2013

The MARGO project also assesses the spatial distribution of the available paleo-data for the deep ocean, such as the $\delta^{18}O$ of benthic foraminifera (Paul and Mulitza, 2009). By all means, the paleo-data coverage is still very sparse compared to the present-day data coverage. Therefore, a powerful data assimilation technique is required to control the model efficiently, given the limited amount of data (Paul and Schäfer-Neth, 2005). In this study, we adopted the constrained least-squares technique for that purpose; namely, we seek a model ocean that corresponds to the minimum value of a so-called objective function, which is mainly the sum of squared differences between data and corresponding model results. This optimised model ocean provides the best estimate for the AMOC and NADW formation rate. The adjoint method (e.g., Wunsch, 1996; Errico, 1997) is a technique to find such an optimised state, because it allows to compute the gradient of the objective function with respect to selected control variables (that may include initial and boundary conditions as well as internal model parameters) and search for its minimum.

Our ultimate goal is to assimilate various paleo-data for the LGM into a numerical ocean model (Paul and Schäfer-Neth, 2005; Schmittner et al., 2011), with the aim of estimating the LGM ocean state as reliably as possible. As the first step, the particular purpose of this paper is to examine whether the spatial distribution and accuracy of the available paleo-data is likely to be adequate to constrain our model properly, and if not, what further data would be required. For this purpose, we used artificial pseudo-proxy data instead of the actual LGM data and estimated the NADW formation rate of a target model ocean from which the pseudo data was sampled. Thereby, we could assess the result of a state estimate exercise by comparing the estimated value with the known "true" value. A feasibility study like this is highly important to evaluate the reliability of a method for state estimation, but nevertheless, it has not been done yet regarding an adjoint-based application to the LGM. The artificial targets had a stronger or weaker NADW formation rate than the reference state to serve as potential analogues for the LGM ocean. The basic set of pseudo-proxy data had the same spatial distribution and

GMDD
6, 4417–4445, 2013

error estimates as the MARGO data, to imitate the quality and quantity of actual paleo-data.

2 Methods

We used the Massachusetts Institute of Technology general circulation model (MITgcm), a state-of-the-art model suitable for ocean state estimation. Here, it was configured to solve the Boussinesq, hydrostatic Navier–Stokes equations (Marshall et al., 1997). Subgrid-scale mixing was parameterised (Gent and McWilliams, 1990). A dynamic-thermodynamic sea-ice model was coupled to the ocean model (Losch et al., 2010). We used a cubed-sphere grid system that avoided converging grid lines and pole singularities (Adcroft et al., 2004) and had six faces, each of which has 32×32 horizontal grid cells, and 15 vertical layers.

The MITgcm can be fitted to data by solving a least-squares problem using the Lagrange multiplier method. For this purpose, the computer code can be differentiated by automatic differentiation (AD) using the source-to-source compiler TAF (Giering and Kaminski, 1998; Heimbach et al., 2005) to generate exact and efficient "adjoint" model code.

For the experiments with artificial pseudo-proxy data (hereafter, referred as pseudo-proxy experiments), we ran the MITgcm forward in time to generate five different model ocean states. One of them was the reference state and at the same time the starting point of all optimisations, and the other four were divided into sets of two that were very different from the reference state by changing the atmospheric boundary conditions (Targets 1 and 2) and the others that were quite similar, but with systematic biases due to modified internal model parameters (Targets 3 and 4, see also Table 1 and Fig. 1).

For the reference state, the model was spun-up from present-day salinity and temperature (Levitus, 1982) for 800 model years from rest with the external forcings based on the protocol of the Coordinated Ocean-ice Reference Experiments (CORE) project (Griffies et al., 2009). We used a tracer acceleration method with a time step of 1 day

GMDD
6, 4417–4445, 2013

for the tracer equations and 20 min for the momentum equations. The maximum of the Atlantic meridional overturning stream function of 18.3 Sv was taken as a measure of the rate of NADW formation in the reference state.

The reference configuration was modified considerably to generate Targets 1 and 2. In both runs the prescribed atmospheric fields were replaced by fields from a coupled atmospheric energy-moisture balance model (Ashkenazy et al., 2013). These simulations corresponded to very different climates mostly as a consequence of the dynamic interaction of the ocean with the atmosphere, although some of the internal ocean model parameters were also modified (Table 2). After another spin-up of 2000 yr we added freshwater to the North Atlantic Ocean uniformly between 20° N and 50° N at a rate of 0.28 Sv for an additional 1000 yr run. We calculated the Atlantic meridional overturning streamfunction and took the maximum of 11.4 Sv as an indication of a reduced rate of NADW formation for Target 1 as compared to the reference state. The unmodified run with an increased rate of 23.7 Sv became Target 2.

Targets 3 and 4 were generated by increasing or reducing internal physical parameters that determine the lateral eddy viscosity for additional 200 yr runs from the reference. These parameters for harmonic and bi-harmonic viscosity (A_h^*, A_4^*) were not used as standard control variables in our experiments. Increasing the eddy-viscosity led to a smaller overturning rate of 12.5 Sv (Target 3) as compared to the reference state, decreasing to a larger overturning rate of 22.9 Sv (Target 4).

Targets 1 and 3 had similarly small NADW formation rates and Target 2 and 4 similarly large rates, but Targets 1 and 2 were much colder than the reference and Targets 3 and 4 (Table 2).

The temperature and salinity distributions of each target were sampled and averaged over the last 10 yr of the simulations. Surface data (SST and SSS) were taken from the top grid nodes, deep-ocean data from the bottom grid nodes. Normally-distributed noise with a standard deviation of the prior errors was added as a random error to obtain the pseudo data. Note that large uncertainties were associated with proxy data so that the prior errors (see below) could be large. This led to the realistic situation that

GMDD
6, 4417–4445, 2013

the proxy data could be strongly biased after adding large noise contributions on the order of, say, 1 °C.

Starting from the reference run, the ocean model was fitted to the pseudo-proxy data by minimizing the following objective function J:

$$J = (\mathbf{T}_{\text{model}} - \mathbf{T}_{\text{target}})^{\mathrm{T}} \mathbf{W}_{\mathrm{t}} (\mathbf{T}_{\text{model}} - \mathbf{T}_{\text{target}}) + (\mathbf{S}_{\text{model}} - \mathbf{S}_{\text{target}})^{\mathrm{T}} \mathbf{W}_{\mathrm{s}} (\mathbf{S}_{\text{model}} - \mathbf{S}_{\text{target}}) , \quad (1)$$

where $\mathbf{T}_{\text{model}}$ and $\mathbf{S}_{\text{model}}$ were the average over the last 10 yr of a 20 yr integration (for each iteration) of temperature and salinity, $\mathbf{T}_{\text{target}}$ and $\mathbf{S}_{\text{target}}$ were pseudo-proxy data based on the artificial targets, $\mathbf{W}_{\mathrm{t}}$ and $\mathbf{W}_{\mathrm{s}}$ were weight matrices that were the inverse of the error covariance matrices. All errors were assumed to be uncorrelated, so that the inverse error covariances reduced to scalar weights. To reconstruct the targets, we used the following control variables: the radiative and wind forcing at the sea surface, the air temperature, the humidity above the sea surface, the precipitation, and the initial temperature and salinity. Every control variable was normalized according to the characteristic scale of each variable, and was smoothed with the 9-point smoothing scheme. A quasi-Newton algorithm (Gilbert and Lemaréchal, 1989) was used to iteratively find optimized control variables that minimize J. The essential gradient information was provided by the adjoint model.

To explore the potential information content of the MARGO data set (Table 1), the first experiments with Targets 1 and 2 only used the model SST sampled at the MARGO core locations as pseudo-proxy data. For these data, we used prior data errors derived from the uncertainty estimated for each individual data point by the MARGO project (Margo Project Members et al., 2009). If a model grid cell contained more than one data point, the weighted average of all data points was used.

Then we successively added hypothetical data sets to improve the data coverage and to assess its effect on the state estimates. We assigned prior errors to the hypothetical data points as specified below.

GMDD
6, 4417–4445, 2013

3 Results

Table 1 summarises the experiments. Those experiments for which the NADW formation rate was adjusted by the least-squares fit to be closer to the target than half of the difference between the starting point (reference state) and target were marked as successful in reconstructing the overturning. These were experiments E1-4 and E1-7 for Target 1 and E2-6 for Target 2. For Targets 3 and 4 experiments except for E4-1 and E4-2 were successful by this measure. The other experiments had either far too large overturning rates or the overturning rate was not affected by the constraining observations.

For the two targets with a much colder climate (Targets 1 and 2) the results were very inconsistent. Surface data of temperature (E1-1 and E2-1) and salinity (E1-3 and E2-3) alone did not appear to be sufficient to constrain the overturning rate. Instead, assimilating these data led to much too strong overturning in all cases; even for Target 1 where the sampled surface data corresponded to a weaker overturning rate. Temperature data alone at the surface and near the bottom were also without effect. In these runs (E1-2 and E2-2), the overturning rate hardly changed relative to the initial guess. Temperature and salinity data near the bottom were required to bring down the overturning rate to the target value in E1-4, or to enhance it in E2-4 although they led to a too strong overturning. Large effect of salinity data on the NADW formation rate was clearly seen in the comparison between E1-2 and E1-4, and between E2-2 and E2-4.

In runs E1-5 and 6 and E2-5 and 6 we assumed that the data were available at all surface grid points. Even for this unrealistically optimistic scenario the agreement of the overturning rates was disappointing. Only with both temperature and salinity data at all surface grid points, one experiment (E2-6) was successful in reproducing the larger overturning rate of Target 2.

If we were able to increase the data accuracy, for example, by increasing the number of observations within a grid cell or by inventing new proxies that would yield a more

GMDD
6, 4417–4445, 2013

accurate reconstruction of temperature and salinity, we could hope to improve the state estimates. In the experiments E1-7 accurate temperature data alone was sufficient for a good agreement of the overturning rate to Target 1. The same configuration led to an adjustment with the wrong sign in E2-7. Accurate temperature and salinity data marginally improved the agreement with the targets' overturning rates compared to other experiments, but not sufficiently to be called successful.

For the second set of targets (Targets 3 and 4) the first-guess atmospheric forcing was the same as for the reference state, but internal model parameters were modified to mimic inherent model biases. Twin experiments, in which the control parameters consisted of just these modified viscosity parameters, confirmed that the system was able to completely remove these biases, if their sources were known (not shown). For the standard control variables (initial conditions and atmospheric forcing fields, see above), the first pair of experiments for Target 3 and 4 (E3-1 and E4-1) seemingly ensured that, providing that the targets were close enough to the reference (i.e., the first guess) with regard to the temperature (Table 1), the same data distribution and errors as those for E1-1 and E2-1 were adequate to guide the NADW formation rates to the right direction even if the target rates were much different from that of the reference state. With much smaller data prior errors (E4-2), the estimated NADW formation rate for Target 4 was better estimated compared to E4-1, although E3-2 was slightly worse than E3-1. For the last two experiments (E3-3 and E4-3) we reduced the control space to the initial conditions, the surface wind stress and the incoming shortwave and longwave radiative fluxes (i.e., reducing the number of control variables from nine into six, which made the model less flexible. also see Sect. 4.2). Even without the air temperature, the humidity, and the precipitation as control variables, the NADW formation rates were successfully estimated.

GMDD
6, 4417–4445, 2013

4 Discussion

4.1 Analyses of the results for Targets 1 and 2

To analyse the differences between the successful and the unsuccessful experiments, we examined the mixed layer depth (MLD) and the location of deep convection in the high-latitude Northern Atlantic in some of the experiments (Figs. 2 and 4). Different rates of NADW formation during the LGM have been suggested to be associated with a shift in the location of deep convection (e.g., Rahmstorf, 1994; Ganopolski and Rahmstorf, 2001; Oka et al., 2012). In the experiments that succeeded in estimating the NADW formation rate for Target 1 (e.g., E1-4), the MLD shoaled from the reference state as for Target 1 (Fig. 2a). Experiments that failed in reconstructing the weaker NADW formation rate had a much deeper MLD compared to the reference (E1-1, 2, 6 in Fig. 2a). This was consistent with too strong NADW formation rates in the reconstructions; especially for the experiments with a very strong NADW formation rate (E1-1). Further, the deep MLD was also found in untypical places (south of Iceland).

The MLD of the state estimates was related to the temperature in the deep ocean. While the temperature field at 1000 m depth for E1-4 was similar to the target temperature (Fig. 2b), the deep ocean was too warm in the other three experiments, especially in E1-1 and E1-6, providing extra buoyancy to favour instability and deep convection. Similarly, the deep ocean salinity at 1000 m depth was too high in the other experiments as compared to E1-4 (Fig. 2d). On the other hand, the temperature field (Fig. 2c) and the salinity fields (Fig. 2e) at 3000 m clearly distinguished E1-4 and E1-2 from E1-1 and E1-6. This was related by the vertical distribution of the data in the North Atlantic Ocean (Fig. 3). Because a relatively large number of deep ocean data were located around at 3000 m depth, the reconstructions at those depths were greatly affected by whether the deep ocean data were used or not for the state estimation. These results suggested that (1) data in the deep ocean were required to constrain the structure of the deep ocean properly; (2) although temperature data for the deep ocean may suffice to some extent, salinity data would still be required for a successful estimate. Note

GMDD
6, 4417–4445, 2013

that temperature and salinity data of the deep ocean were also used in E1-6, but their contribution was very small, because the weight of the deep-ocean data decreased relative to the surface-ocean data in proportion of the number of data points.

For Target 2, experiments E2-6, which successfully reproduced the stronger NADW formation rate, and E2-8 showed a similar MLD anomaly with respect to the target (Fig. 4a – albeit the positive anomalies in E2-8 were too large corresponding to the too high rate of NADW formation rate in this experiment). However, in E2-7, the region of the positive MLD anomaly was restricted to a small area, causing a much weaker NADW formation rate than in the target. As expected from the data used in those three experiments, the sea-surface salinity (SSS) was very different for E2-7 compared to E2-6 and E2-8 (Fig. 4b). The low SSS of E2-7 caused the low density of sea water that stabilised the water column and reduced deep mixing. In addition to the results for Target 1, these results also supported that the salinity data was required for successful estimates.

We note that the principal location of deep convection of Target 2 (the south-east of Iceland) was successfully predicted in every experiment (i.e., irrespective of the NADW formation rate). As for Target 1, although the shifts in the location of deep convection were also observed in all experiments, only some experiments succeeded in predicting exactly the locations of the target. But those experiments did not necessarily reconstruct the proper NADW formation rate. These results suggested that predicting the MLD was not equivalent to predicting the location of deep convection. It was the MLD that was better correlated with the NADW formation rate.

4.2 Outlook for reconstructions with a better first guess

The experiments for Targets 1 and 2 demonstrated that the targets were not consistently reconstructed, even when we assumed very optimistic conditions for data quality and quantity, and in spite of the fact that the atmospheric state that was responsible for the differences was part of the control vector and was adjusted in the optimisation process. The results suggested that it was difficult with the available data to "pull"

GMDD
6, 4417–4445, 2013

the model towards targets that were very different from the first guess. Providing prior knowledge, that is, a better first guess may alleviate the problem as illustrated in the following. We remind the reader that for Targets 3 and 4 internal friction parameters were modified that were not part of the control vector. This choice introduced a model bias that could not be adjusted by the assimilation in the "correct" way, a situation that is definitely encountered in every state estimation exercise.

In all three pairs of experiments for Target 3 and 4 the NADW formation rate had the correct direction of deviation from the initial guess. However, there were large differences among the temperature fields of those experiments (Fig. 5). The SST fields of E3-1 and E4-1 were very different from those of their respective target fields (third column in Fig. 5), because the noisy pseudo data to which the model adjusted was also very different from the original targets because of the large associated uncertainty (second column of Fig. 5). The experiments with very small data errors and accordingly reduced noise in the data (E3-2 and E4-2) did not have this problem and hence the agreement between model and target was much better (fourth column in Fig. 5). The experiments with fewer control variables (E3-3 and E4-3, fifth column in Fig. 5) avoided the overfitting to data of poor quality (i.e., data with a low signal-to-noise ratio) by using a less flexible model that restricted the departure from the first guess. This amounted to providing even more prior knowledge, as we assumed implicitly that air temperature, humidity and precipitation were well known.

The good NADW reconstruction in E3-3 and E4-3 was connected to the modified freshwater flux in the high-latitude North Atlantic (Fig. 6a). Note that the surface freshwater flux was not part of the control vector in this case. Instead, changes in the surface freshwater flux were caused by adjustments of the incoming radiative fluxes that led to changes in temperature and thus to changes in evaporation. For E3-3, this positive freshwater flux anomaly, consistent with the difference in freshwater flux between the target and the reference state, stabilised the water column and inhibited NADW formation. In contrast, a negative freshwater anomaly destabilised the water column and led to increased NADW formation in E4-3. The difference between the target and the

GMDD
6, 4417–4445, 2013

reference state was also generally negative. Similar patterns of the SST and freshwater flux anomalies (Fig. 5b) show that the evaporation rate was strongly controlled by the SST. Consequently, adjusting the SST in the high-latitude North Atlantic to the target values led to a successful reconstruction of the NADW formation rate. By way of this freshwater flux anomaly, the SST adjustment roughly reproduced the sea-surface salinity (SSS) without using SSS as a constraint (Fig. 5c), because the SSS anomalies in the targets were also, in part, caused by the change in evaporation due to SST changes.

5 Conclusions

Can we use sparse paleoceanographic proxy data to reconstruct the strength of the AMOC during the LGM, using the MITgcm? Our answer is two-fold: (1) with a sufficiently good first guess, one can indeed reconstruct the strength of the AMOC from sparse sea-surface temperature data such as the existing MARGO data set. (2) Otherwise, however, one needs in addition deep-ocean temperature data, sea-surface and deep-ocean salinity data (or any other data that allows to infer paleo-ocean density), and smaller data uncertainty.

Although a good first guess with a reasonable representation of past hydrographic conditions would be very helpful, finding such a first guess is essentially part of the state estimation that we are aiming for. A further problem to be addressed is overfitting the model to data with a poor signal-to-noise ratio. Both issues could be addressed by adding either more data (once available) or prior knowledge. One way of adding prior knowledge would be re-considering the control parameter space and adding more model physics. In particular, the surface fluxes could be more physically constrained by coupling the ocean model to an atmospheric model, for example, an energy-moisture balance model (e.g. Ashkenazy et al., 2013). Using such a model could also enable more control over the global SST by changing, for example, the CO_2 content of the atmosphere, the planetary albedo or the atmospheric heat transport efficiency (Paul

GMDD
6, 4417–4445, 2013

and Losch, 2012), and at the same time decrease the degrees of freedom of the model by reducing the control variables.

Another more direct but less physical way to add prior knowledge is to enforce smoothness through a Laplacian of some physical quantity (e.g. surface temperature) or to penalise deviations from the first guess; this, however, is only possible at the cost of introducing more biases.

The integration period in our experiments was chosen for purely economical reasons, and our simulations were not long enough to guarantee stable steady state solutions. Cost function terms that penalise inter-annual variations could be used to enforce a steady state. Alternatively, longer integration periods for each iteration would be required. Paleo data from regions where Antarctic Bottom Water is formed may become more important on longer time scales, because the relative densities of the North Atlantic and Southern Ocean source waters are expected to play a larger role for the meridional overturning circulation in the steady-state problem (Paul and Schäfer-Neth, 2003).

Acknowledgements. This research was funded by the DFG-Research Center/Center of Excellence MARUM – "The Ocean in the Earth System". The adjoint model was generated with TAF (Giering and Kaminski, 1998).

References

Adcroft, A., Campin, J.-M., Hill, C., and Marshall, J.: Implementation of an atmosphere ocean general circulation model on the expanded spherical cube, Mon. Weather Rev., 132, 2845, doi:10.1175/MWR2823.1, 2004. 4422

Adkins, J. F., McIntyre, K., and Schrag, D. P.: The salinity, temperature, and $\delta^{18}O$ of the glacial deep ocean, Science, 298, 1769–1773, doi:10.1126/science.1076252, 2002. 4420

Archer, D.: Modeling the calcite Lysocline, J. Geophys. Res., 96, 17037, doi:10.1029/91JC01812, 1991. 4419

GMDD

6, 4417–4445, 2013

Archer, D., Winguth, A., Lea, D., and Mahowald, N.: What caused the glacial/interglacial atmospheric pCO_2 cycles?, Rev. Geophys., 38, 159–189, doi:10.1029/1999RG000066, 2000. 4419

Ashkenazy, Y., Losch, M., Gildor, H., Mirzayof, D., and Tziperman, E.: Multiple sea-ice states and abrupt MOC transitions in a general circulation ocean model, Climate Dynam., 40, 1803–1817, doi:10.1007/s00382-012-1546-2, 2013. 4423, 4430

Clark, P. U., Marshall, S. J., Clarke, G. K. C., Hostetler, S. W., Licciardi, J. M., and Teller, J. T.: Freshwater forcing of abrupt climate change during the last glaciation, Science, 293, 283–287, doi:10.1126/science.1062517, 2001. 4418

Curry, W. B. and Oppo, D. W.: Glacial water mass geometry and the distribution of $\delta^{13}C$ of ΣCO_2 in the western Atlantic Ocean, Paleoceanography, 20, PA1017, doi:10.1029/2004PA001021, 2005. 4420

Dail, H. J.: Atlantic Ocean Circulation at the Last Glacial Maximum: Inferences from Data and Models, Ph. D. thesis, Massachusetts Institute of Technology, Massachusetts and the Woods Hole Oceanographic Institution, Massachusetts, 2012. 4420

Epica Community Members, Barbante, C., Barnola, J.-M., Becagli, S., Beer, J., Bigler, M., Boutron, C., Blunier, T., Castellano, E., Cattani, O., Chappellaz, J., Dahl-Jensen, D., Debret, M., Delmonte, B., Dick, D., Falourd, S., Faria, S., Federer, U., Fischer, H., Freitag, J., Frenzel, A., Fritzsche, D., Fundel, F., Gabrielli, P., Gaspari, V., Gersonde, R., Graf, W., Grigoriev, D., Hamann, I., Hansson, M., Hoffmann, G., Hutterli, M. A., Huybrechts, P., Isaksson, E., Johnsen, S., Jouzel, J., Kaczmarska, M., Karlin, T., Kaufmann, P., Kipfstuhl, S., Kohno, M., Lambert, F., Lambrecht, A., Lambrecht, A., Landais, A., Lawer, G., Leuenberger, M., Littot, G., Loulergue, L., Lüthi, D., Maggi, V., Marino, F., Masson-Delmotte, V., Meyer, H., Miller, H., Mulvaney, R., Narcisi, B., Oerlemans, J., Oerter, H., Parrenin, F., Petit, J.-R., Raisbeck, G., Raynaud, D., Röthlisberger, R., Ruth, U., Rybak, O., Severi, M., Schmitt, J., Schwander, J., Siegenthaler, U., Siggaard-Andersen, M.-L., Spahni, R., Steffensen, J. P., Stenni, B., Stocker, T. F., Tison, J.-L., Traversi, R., Udisti, R., Valero-Delgado, F., van den Broeke, M. R., van de Wal, R. S. W., Wagenbach, D., Wegner, A., Weiler, K., Wilhelms, F., Winther, J.-G., and Wolff, E.: One-to-one coupling of glacial climate variability in Greenland and Antarctica, Nature, 444, 195–198, doi:10.1038/nature05301, 2006. 4418

Errico, R. M.: What Is an Adjoint Model?, B. Am. Meteorol. Soc., 78, 2577–2591, doi:10.1175/1520-0477(1997)078<2577:WIAAM>2.0.CO;2, 1997. 4421

GMDD
6, 4417–4445, 2013

Ganopolski, A. and Rahmstorf, S.: Rapid changes of glacial climate simulated in a coupled climate model, Nature, 409, 153–158, doi:10.1038/409153A0, 2001. 4418, 4427

Gebbie, G. and Huybers, P.: Meridional circulation during the Last Glacial Maximum explored through a combination of South Atlantic $\delta^{18}O$ observations and a geostrophic inverse model, Geochem. Geophys. Geosyst., 7, Q11N07, doi:10.1029/2006GC001383, 2006. 4420

Gent, P. R. and McWilliams, J. C.: Isopycnal mixing in ocean circulation models, J. Phys. Oceanogr., 20, 150–160, doi:10.1175/1520-0485(1990)020<0150:IMIOCM>2.0.CO;2, 1990. 4422, 4439

Gent, P. R., Willebrand, J., McDougall, T. J., and McWilliams, J. C.: Parameterizing Eddy-induced tracer transports in ocean circulation models, J. Phys. Oceanogr., 25, 463–474, doi:10.1175/1520-0485(1995)025<0463:PEITTI>2.0.CO;2, 1995. 4439

Giering, R. and Kaminski, T.: Recipes for adjoint code construction, ACM Trans. Math. Softw., 24, 437–474, doi:10.1145/293686.293695, 1998. 4422, 4431

Gilbert, J. C. and Lemaréchal, C.: Some numerical experiments with variable-storage quasi-Newton algorithms, Math. Program., 45, 407–435, doi:10.1007/BF01589113, 1989. 4424

Gildor, H. and Tziperman, E.: Physical mechanisms behind biogeochemical glacial-interglacial CO_2 variations, Geophys. Res. Lett., 28, 2421–2424, doi:10.1029/2000GL012571, 2001. 4419

Griffies, S. M., Biastoch, A., Böning, C., Bryan, F., Danabasoglu, G., Chassignet, E. P., England, M. H., Gerdes, R., Haak, H., Hallberg, R. W., Hazeleger, W., Jungclaus, J., Large, W. G., Madec, G., Pirani, A., Samuels, B. L., Scheinert, M., Gupta, A. S., Severijns, C. A., Simmons, H. L., Treguier, A. M., Winton, M., Yeager, S., and Yin, J.: Coordinated Ocean-ice Reference Experiments (COREs), Ocean Model., 26, 1–46, doi:10.1016/j.ocemod.2008.08.007, 2009. 4422

Heimbach, P., Hill, C., and Giering, R.: An efficient exact adjoint of the parallel MIT general circulation model, generated via automatic differentiation, Future Gener. Comput. Syst., 21, 1356–1371, doi:10.1016/j.future.2004.11.010, 2005. 4422

Keigwin, L. D. and Lehman, S. J.: Deep circulation change linked to HEINRICH Event 1 and Younger Dryas in a middepth North Atlantic Core, Paleoceanography, 9, 185–194, doi:10.1029/94PA00032, 1994. 4418

Kurahashi-Nakamura, T., Abe-Ouchi, A., and Yamanaka, Y.: Effects of physical changes in the ocean on the atmospheric pCO_2: glacial-interglacial cycles, Clim. Dynam., 35, 713–719, doi:10.1007/s00382-009-0609-5, 2010. 4419

GMDD
6, 4417–4445, 2013

Levitus, S. E.: Climatological Atlas of the World Ocean, NOAA Professional Paper 13, US Government Printing Office, Washington DC, 1982. 4422

Lippold, J., Luo, Y., Francois, R., Allen, S. E., Gherardi, J., Pichat, S., Hickey, B., and Schulz, H.: Strength and geometry of the glacial Atlantic Meridional Overturning Circulation, Nat. Geosci., 5, 813–816, doi:10.1038/ngeo1608, 2012. 4419

Losch, M., Menemenlis, D., Campin, J.-M., Heimbach, P., and Hill, C.: On the formulation of sea-ice models. Part 1: Effects of different solver implementations and parameterizations, Ocean Model., 33, 129–144, doi:10.1016/j.ocemod.2009.12.008, 2010. 4422

Lynch-Stieglitz, J., Curry, W. B., and Slowey, N.: A geostrophic transport estimate for the Florida Current from the oxygen isotope composition of benthic foraminifera, Paleoceanography, 14, 360–373, doi:10.1029/1999PA900001, 1999a. 4419

Lynch-Stieglitz, J., Curry, W. B., and Slowey, N.: Weaker Gulf Stream in the Florida Straits during the Last Glacial Maximum, Nature, 402, 644–648, doi:10.1038/45204, 1999b. 4419

Lynch-Stieglitz, J., Curry, W. B., Oppo, D. W., Ninneman, U. S., Charles, C. D., and Munson, J.: Meridional overturning circulation in the South Atlantic at the last glacial maximum, Geochem. Geophys. Geosyst., 7, Q10N03, doi:10.1029/2005GC001226, 2006. 4419

Manighetti, B. and McCave, I. N.: Late Glacial and Holocene palaeocurrents around Rockall Bank, NE Atlantic Ocean, Paleoceanography, 10, 611–626, doi:10.1029/94PA03059, 1995. 4419

Margo Project Members, Waelbroeck, C., Paul, A., Kucera, M., Rosell-Melé, A., Weinelt, M., Schneider, R., Mix, A. C., Abelmann, A., Armand, L., Bard, E., Barker, S., Barrows, T. T., Benway, H., Cacho, I., Chen, M.-T., Cortijo, E., Crosta, X., de Vernal, A., Dokken, T., Duprat, J., Elderfield, H., Eynaud, F., Gersonde, R., Hayes, A., Henry, M., Hillaire-Marcel, C., Huang, C.-C., Jansen, E., Juggins, S., Kallel, N., Kiefer, T., Kienast, M., Labeyrie, L., Leclaire, H., Londeix, L., Mangin, S., Matthiessen, J., Marret, F., Meland, M., Morey, A. E., Mulitza, S., Pflaumann, U., Pisias, N. G., Radi, T., Rochon, A., Rohling, E. J., Sbaffi, L., Schäfer-Neth, C., Solignac, S., Spero, H., Tachikawa, K., and Turon, J.-L.: Constraints on the magnitude and patterns of ocean cooling at the Last Glacial Maximum, Nat. Geosci., 2, 127–132, doi:10.1038/ngeo411, 2009. 4420, 4424

Marshall, J., Adcroft, A., Hill, C., Perelman, L., and Heisey, C.: A finite-volume, incompressible Navier Stokes model for studies of the ocean on parallel computers, J. Geophys. Res., 102, 5753–5766, doi:10.1029/96JC02775, 1997. 4422

GMDD
6, 4417–4445, 2013

McCave, I. N. and Hall, I. R.: Size sorting in marine muds: processes, pitfalls, and prospects for paleoflow-speed proxies, Geochem. Geophys. Geosyst., 7, Q10N05, doi:10.1029/2006GC001284, 2006. 4419

McCave, I. N., Manighetti, B., and Beveridge, N. A. S.: Circulation in the glacial North Atlantic inferred from grain-size measurements, Nature, 374, 149–152, doi:10.1038/374149a0, 1995. 4419

McManus, J. F., Francois, R., Gherardi, J.-M., Keigwin, L. D., and Brown-Leger, S.: Collapse and rapid resumption of Atlantic meridional circulation linked to deglacial climate changes, Nature, 428, 834–837, doi:10.1038/nature02494, 2004. 4419

Mix, A., Bard, E., and Schneider, R.: Environmental processes of the ice age: land, oceans, glaciers (EPILOG), Quaternary Sci. Rev., 20, 627–657, doi:10.1016/S0277-3791(00)00145-1, 2001. 4419

Negre, C., Zahn, R., Thomas, A. L., Masqué, P., Henderson, G. M., Martínez-Méndez, G., Hall, I. R., and Mas, J. L.: Reversed flow of Atlantic deep water during the Last Glacial Maximum, Nature, 468, 84–89, doi:10.1038/nature09508, 2010. 4419

Oka, A., Hasumi, H., and Abe-Ouchi, A.: The thermal threshold of the Atlantic meridional overturning circulation and its control by wind stress forcing during glacial climate, Geophys. Res. Lett., 39, L09709, doi:10.1029/2012GL051421, 2012. 4427

Otto-Bliesner, B. L., Hewitt, C. D., Marchitto, T. M., Brady, E., Abe-Ouchi, A., Crucifix, M., Murakami, S., and Weber, S. L.: Last Glacial Maximum ocean thermohaline circulation: PMIP2 model intercomparisons and data constraints, Geophys. Res. Lett., 34, L12706, doi:10.1029/2007GL029475, 2007. 4420

Paul, A. and Losch, M.: Perspectives of parameter and state estimation in paleoclimatology, in: Climate Change, Proceedings of the Milutin Milankovitch 130th Anniversary Symposium, Part 2, edited by: Berger, A., Mesinger, F., and Šijački, D., 93–105, Springer, Heidelberg, 2012. 4430

Paul, A. and Mulitza, S.: Challenges to understanding ocean circulation during the Last Glacial Maximum, EOS Trans., 90, p. 169, doi:10.1029/2009EO190004, 2009. 4421

Paul, A. and Schäfer-Neth, C.: Modeling the water masses of the Atlantic Ocean at the Last Glacial Maximum, Paleoceanography, 18, 1058, doi:10.1029/2002PA000783, 2003. 4431

Paul, A. and Schäfer-Neth, C.: How to combine sparse proxy data and coupled climate models, Quaternary Sci. Rev., 24, 1095–1107, doi:10.1016/j.quascirev.2004.05.010, 2005. 4421

GMDD
6, 4417–4445, 2013

Piotrowski, A. M., Goldstein, S. L., Hemming, S. R., and Fairbanks, R. G.: Temporal relationships of carbon cycling and ocean circulation at glacial boundaries, Science, 307, 1933–1938, doi:10.1126/science.1104883, 2005. 4419

Rahmstorf, S.: Rapid climate transitions in a coupled ocean-atmosphere model, Nature, 372, 82–85, doi:10.1038/372082a0, 1994. 4427

Redi, M. H.: Oceanic isopycnal mixing by coordinate rotation, J. Phys. Oceanogr., 12, 1154–1158, doi:10.1175/1520-0485(1982)012<1154:OIMBCR>2.0.CO;2, 1982. 4439

Rohling, E. J.: Paleosalinity: confidence limits and future applications, Mar. Geol., 163, 1–11, doi:10.1016/S0025-3227(99)00097-3, 2000. 4420

Rutberg, R. L. and Peacock, S. L.: High-latitude forcing of interior ocean $\delta^{13}C$, Paleoceanography, 21, PA2012, doi:10.1029/2005PA001226, 2006. 4420

Schmidt, G. A.: Error analysis of paleosalinity calculations, Paleoceanography, 14, 422–429, doi:10.1029/1999PA900008, 1999. 4420

Schmittner, A., Urban, N. M., Shakun, J. D., Mahowald, N. M., Clark, P. U., Bartlein, P. J., Mix, A. C., and Rosell-Melé, A.: Climate sensitivity estimated from temperature reconstructions of the last glacial maximum, Science, 334, 1385–1388, doi:10.1126/science.1203513, 2011. 4421

Schulz, M., Seidov, D., Sarnthein, M., and Stattegger, K.: Modeling ocean-atmosphere carbon budgets during the Last Glacial Maximum-Heinrich 1 meltwater event-Bølling transition, Int. J. Earth Sci., 90, 412–425, doi:10.1007/s005310000136, 2001. 4419

Solomon, S., Dahe, Q., and Manning, M.: Technical summary, in: Climate Change 2007, Contribution of Working Group I to the Fourth Assessment Report of the Intergovernmental Panel on Climate Change, edited by: Solomon, S., Qin, D., Manning, M., Chen, Z., Marquis, M., Averyt, K. B., Tignor, M., and Miller, H. L., 19–91, Cambridge Univ. Press, Cambridge, 2007. 4419

Stocker, T. F. and Johnsen, S. J.: A minimum thermodynamic model for the bipolar seesaw, Paleoceanography, 18, 1087, doi:10.1029/2003PA000920, 2003. 4418

Visbeck, M., Marshall, J., Haine, T., and Spall, M.: Specification of eddy transfer coefficients in coarse-resolution ocean circulation models, J. Phys. Oceanogr., 27, 381–401, 1997. 4439

Winguth, A. M. E., Archer, D., Duplessy, J.-C., Maier-Reimer, E., and Mikolajewicz, U.: Sensitivity of paleonutrient tracer distributions and deep-sea circulation to glacial boundary conditions, Paleoceanography, 14, 304–323, doi:10.1029/1999PA900002, 1999. 4420

GMDD
6, 4417–4445, 2013

Winguth, A. M. E., Archer, D., Maier-Reimer, E., and Mikolajewicz, U.: Paleonutrient data analysis of the glacial Atlantic using an adjoint ocean general circulation model, Washington DC American Geophysical Union Geophysical Monograph Series, 114, 171–183, doi:10.1029/GM114p0171, 2000. 4420

Wunsch, C.: The Ocean Circulation Inverse Problem, Cambridge University Press, Cambridge, 1996. 4421

Yu, E.-F., Francois, R., and Bacon, M. P.: Similar rates of modern and last-glacial ocean thermohaline circulation inferred from radiochemical data, Nature, 379, 689–694, doi:10.1038/379689a0, 1996. 4419

GMDD
6, 4417–4445, 2013

Table 1. Summary of experiment settings and results. Used data are specified as follows. ST: surface temperature from MARGO data locations, DT: Deep temperature from MARGO data locations, AST: surface temperature from all other grid cells, SS: surface salinity from MARGO data locations, DS: deep salinity from MARGO data locations, ASS: surface salinity from all other grid cells. Maximum values of the AMOC stream function are shown in Sv (1 Sv = 10^6 m^3 s^{-1}). Reconstructed AMOC strength that is closer to the target than half of the difference between the starting point (reference state) and target is shown in italics.

Experiment	Used data						Data errors	Maximum of AMOC stream function (Sv)
	ST	DT	AST	SS	DS	ASS		
Reference state								**18.3**
Target 1								**11.4**
E1-1	x						MARGO	39.1
E1-2	x	x					MARGO/σ = 2.0	19.5
E1-3	x			x			MARGO	31.4
E1-4	x	x		x	x		MARGO/σ = 2.0	*13.8*
E1-5	x	x	x				MARGO/σ = 2.0	20.3
E1-6	x	x	x	x	x	x	MARGO/σ = 2.0	21.5
E1-7	x	x					σ = 0.1	*14.2*
E1-8	x	x		x	x		σ = 0.1	16.1
Target 2								**23.7**
E2-1	x						MARGO	30.5
E2-2	x	x					MARGO/σ = 2.0	18.9
E2-3	x			x			MARGO	43.8
E2-4	x	x		x	x		MARGO/σ = 2.0	37.4
E2-5	x	x	x				MARGO/σ = 2.0	18.8
E2-6	x	x	x	x	x	x	MARGO/σ = 2.0	*24.9*
E2-7	x	x					σ = 0.1	14.6
E2-8	x	x		x	x		σ = 0.1	29.5
Target 3								**12.5**
E3-1	x						MARGO	*13.7*
E3-2	x						σ = 0.1	*14.3*
E3-3	x						MARGO	*14.9*
Target 4								**22.9**
E4-1	x						MARGO	30.2
E4-2	x						σ = 0.1	20.2
E4-3	x						MARGO	*21.8*

GMDD
6, 4417–4445, 2013

Table 2. Summary of model configurations for the reference state and the targets. 1: Redi (1982); Gent and McWilliams (1990); Gent et al. (1995). 2: Visbeck et al. (1997).

Parameters	Reference	Target 1	Target 2	Target 3	Target 4
Normalized lateral eddy viscosity A_h^* (non-dim.)	1.2×10^{-2}	0	0	1.5×10^{-2}	5.0×10^{-3}
Normalized biharmonic viscosity A_4^* (non-dim.)	1.2×10^{-1}	3.0×10^{-1}	3.0×10^{-1}	1.5×10^{-1}	5.0×10^{-2}
Vertical eddy viscosity (r^2/s)	1.0×10^{-3}	1.0×10^{-3}	1.0×10^{-3}	1.0×10^{-3}	1.0×10^{-3}
Vertical diffusion coefficient (m^2/s)	3.0×10^{-5}	3.0×10^{-5}	3.0×10^{-5}	3.0×10^{-5}	3.0×10^{-5}
Parameterization scheme for vertical mixing	implicit vertical diffusion	Nonlocal K-Profile Parameterization (KPP)	Nonlocal K-Profile Parameterization (KPP)	implicit vertical diffusion	implicit vertical diffusion
Parameterization scheme for geostrophic eddies	Redi/GM parameterization[1]	GM with variable eddy coefficients[2]	GM with variable eddy coefficients[2]	Redi/GM parameterization[1]	Redi/GM parameterization[1]
Mean absolute deviation of sea surface temperature (SST) from the reference	–	2.9 K	2.9 K	0.14 K	0.16 K
Root mean square of SST difference from the reference	–	3.5 K	3.4 K	0.3 K	0.3 K

[1]: Redi (1982); Gent and Williams (1990); Gent et al. (1995)
[2]: Visbeck et al. (1997)

GMDD
6, 4417–4445, 2013

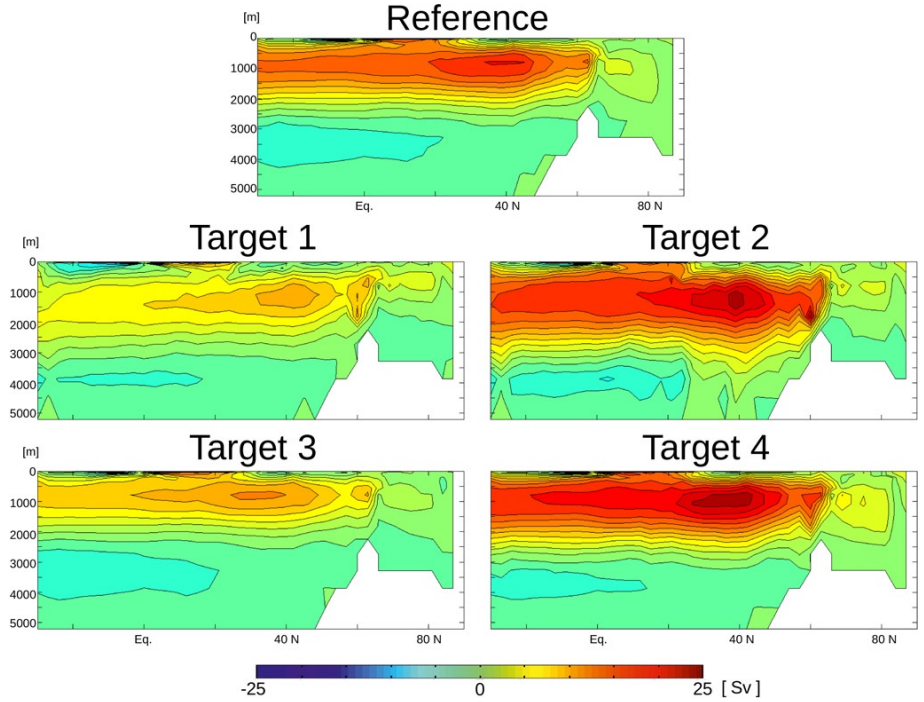

Fig. 1. Stream function of the Atlantic meridional overturning circulation for the reference state and the four targets.

GMDD
6, 4417–4445, 2013

Ocean reconstruction from sparse data

T. Kurahashi-Nakamura et al.

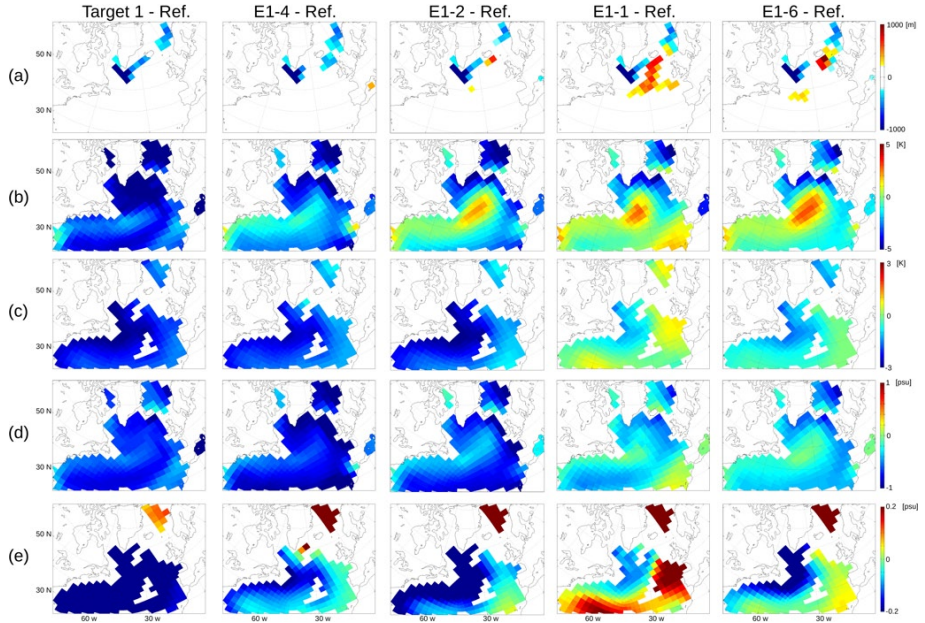

Fig. 2. Anomalies in Target 1, E1-4, E1-2, E1-1, and E1-6 compared to the reference state: the mixed layer depth **(a)**, the temperature at the depth of 1000 m **(b)** and 3000 m **(c)**, and the salinity at the depth of 1000 m **(d)** and 3000 m **(e)**.

GMDD
6, 4417–4445, 2013

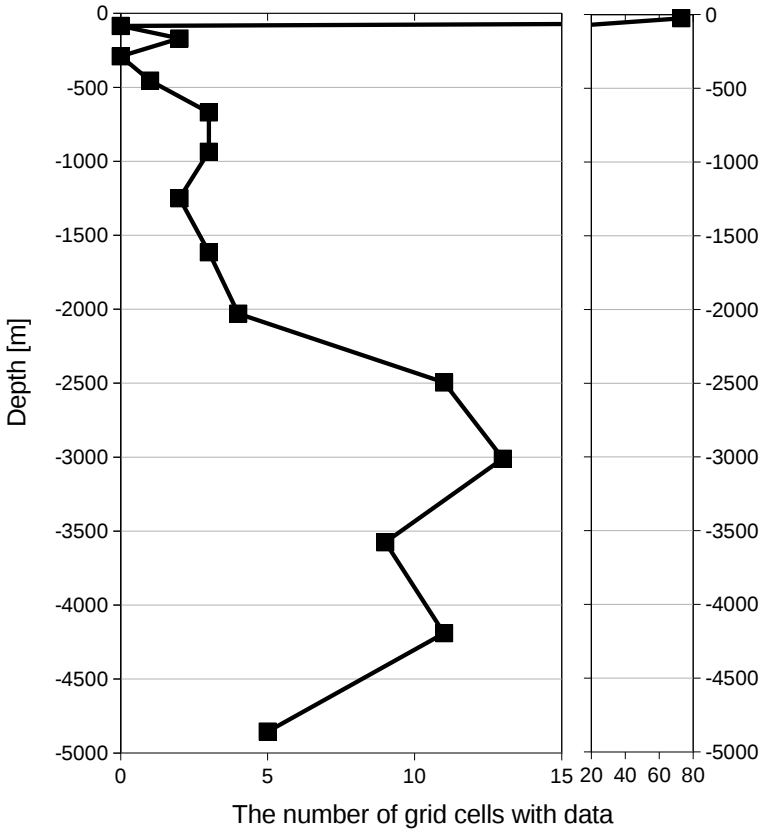

Fig. 3. Vertical distribution of the data in the Northern Atlantic Ocean. The number of grid cells that contain any data in the domain illustrated in Fig. 2 is shown as a function of depth.

GMDD
6, 4417–4445, 2013

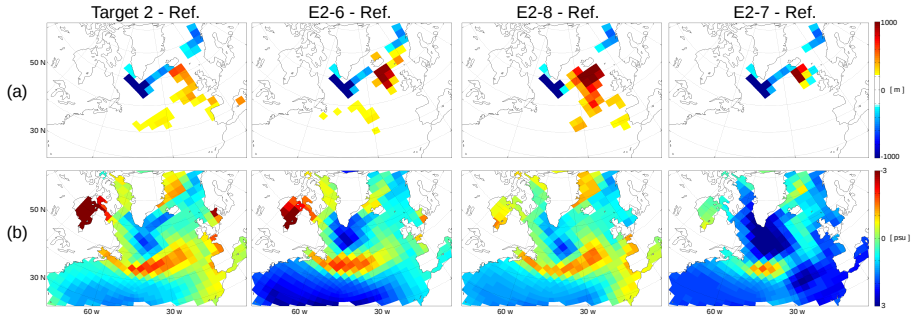

Fig. 4. Anomalies in Target 2, E2-6, E2-8, and E2-7 compared to the reference state: the mixed layer depth **(a)**, and the sea surface salinity **(b)**.

GMDD
6, 4417–4445, 2013

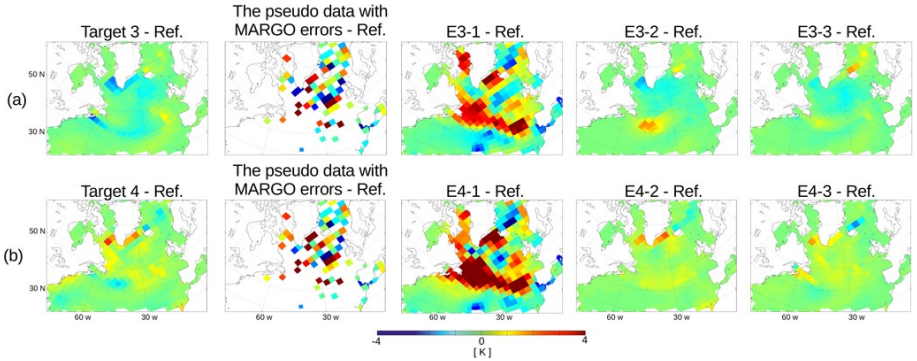

Fig. 5. Anomalies of the sea surface temperature compared to the reference state in Target 3, the pseudo data with the MARGO errors, E3-1, E3-2, and E3-3 **(a)**, and Target 4, the pseudo data, E4-1, E4-2, and E4-3 **(b)**.

GMDD
6, 4417–4445, 2013

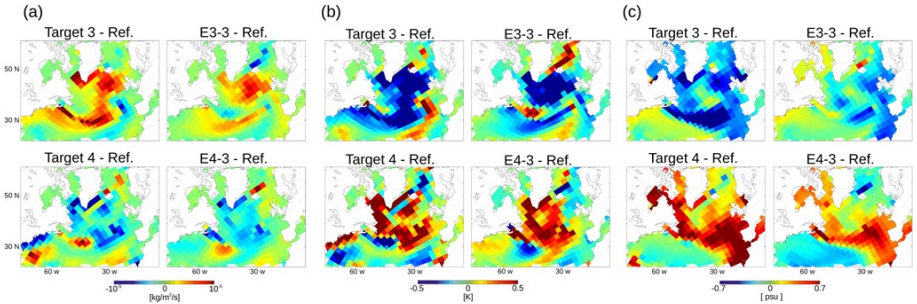

Fig. 6. Anomalies in Target 3, E3-3, Target 4, and E4-3 compared to the reference state: the fresh-water flux **(a)**, the sea surface temperature **(b)**, and the sea surface salinity **(c)**.

GMDD
6, 4417–4445, 2013